Journal of Biomolecular NMR (2019) 73:461–469
https://doi.org/10.1007/s10858-019-00244-6

ARTICLE

Exchange saturation transfer and associated NMR techniques for studies of protein interactions involving high-molecular-weight systems

Vitali Tugarinov[1] · **G. Marius Clore**[1]

Received: 21 February 2019 / Accepted: 27 March 2019 / Published online: 12 August 2019

Abstract
A brief overview of theoretical and experimental aspects of the Dark state Exchange Saturation Transfer (DEST) and lifetime line broadening (ΔR_2) NMR methodologies is presented from a physico-chemical perspective. We describe how the field-dependence of ΔR_2 can be used for determining the exchange regime on the transverse spin relaxation time-scale. Some limitations of DEST/ΔR_2 methodology in applications to molecular systems with intermediate molecular weights are discussed, and the means of overcoming these limitations via the use of closely related exchange NMR techniques is presented. Finally, several applications of DEST/ΔR_2 methodology are described from a methodological viewpoint, with an emphasis on providing examples of how kinetic and relaxation parameters of exchange can be reliably extracted from the experimental data in each particular case.

Keywords Dark state exchange saturation transfer · Lifetime line broadening · Exchanging systems · High molecular weight

Dark state Exchange Saturation Transfer (DEST) and lifetime line broadening (ΔR_2) methodologies, introduced about 8 years ago, have provided a powerful means of investigating exchange processes involving very high-molecular weight species by NMR (Fawzi et al. 2010, 2011, 2012; Anthis and Clore 2015). Examples include early stages of peptide/protein aggregation processes (Fawzi et al. 2010, 2011, 2014; Conicella and Fawzi 2014), binding of peptides to and protein folding on large supra-molecular machines such as the chaperonin GroEL (Libich et al. 2013, 2015, 2017; Wälti et al. 2018), and interactions of proteins and peptides with nanoparticles (Ceccon et al. 2014, 2016a,b, 2017, 2018a, b, 2019; Egner et al. 2017). Dennis Torchia, to whom this brief review is dedicated on the occasion of his 80th birthday, played an important role in the initial stages of development of these NMR techniques (Fawzi et al. 2010, 2011, 2012). Dennis's profound knowledge of NMR theory in general and of NMR applications for the studies of chemical exchange processes in particular, proved invaluable for laying the groundwork for the development of these NMR methods, as well as a theoretically sound interpretation of early-stage experimental results.

In recognition of Dennis's extensive contributions to the field of exchange NMR, as well as his role in the development of DEST/ΔR_2 methodology, here we provide a brief overview of NMR developments in studies of exchange processes involving high-molecular-weight systems with a special emphasis on the physico-chemical aspects of the methodology. This account is therefore not intended to survey in detail all the applications of the DEST/ΔR_2 methodology that have appeared in the scientific literature in recent years, but rather focuses on certain quantitative aspects of DEST/ΔR_2 and associated NMR techniques. We anticipate that our treatment of some of the NMR nuances of this methodology will be useful for those NMR researchers actively engaged in studying chemical exchange processes involving high-molecular-weight systems.

We start with a description of the theoretical underpinnings of exchange-induced lifetime line broadening (ΔR_2)

✉ Vitali Tugarinov
vitali.tugarinov@nih.gov

✉ G. Marius Clore
mariusc@mail.nih.gov

[1] Laboratory of Chemical Physics, National Institute of Diabetes and Digestive and Kidney Diseases, National Institutes of Health, Bethesda, MD 20892-0520, USA

and describe how the field-dependence of ΔR_2 can be used to determine the exchange regime on the transverse spin relaxation time-scale. In what follows, we describe some limitations of DEST/ΔR_2 methodology in applications to molecular systems with intermediate molecular weights (and hence transverse spin relaxation rates), and delineate the means of overcoming these limitations by supplementing DEST and ΔR_2 data with data obtained from closely related NMR techniques. Finally, several applications of DEST/ΔR_2 methodology are described from a methodological perspective with an emphasis on providing examples of how the kinetic and relaxation parameters of exchange can be reliably and unambiguously extracted from the NMR data in each particular case.

Lifetime line broadening, chemical exchange-induced line broadening and chemical shifts

The magnetization of a molecular system exchanging between two states A and B with first-order rate constants k_a and k_b, $A \underset{k_b}{\overset{k_a}{\rightleftarrows}} B$, evolves according to,

$$\frac{d}{dt}\begin{bmatrix} M^A \\ M^B \end{bmatrix} = -\begin{bmatrix} R_2^A + k_a & -k_b \\ -k_a & R_2^B + k_b + i\Delta\omega \end{bmatrix}\begin{bmatrix} M^A \\ M^B \end{bmatrix} \quad (1)$$

where M^A and M^B are the transverse magnetization operators of states A and B, respectively; R_2^A and R_2^B are the respective intrinsic transverse relaxation rates of the two states in the absence of exchange; and $\Delta\omega$ is the difference in chemical shifts $(\omega_B - \omega_A)$ between states A and B (in rad/s), where the on-resonance condition with respect to state A is assumed $(\omega_A = 0)$. In the context of molecular association, k_a is a pseudo-first order ('apparent') association rate constant, k_{on}^{app}, and k_b is the first-order dissociation rate constant, k_{off}. Exact analytical solutions of the differential equations given by Eq. 1 are straightforward to obtain. However, simple approximations for chemical exchange line broadening, R_{ex}, and the exchange-induced chemical shift, δ_{ex}, can be derived under conditions where the populations of states A and B are highly skewed ($k_b >> k_a$). Retaining only the leading term in the characteristic polynomial, and taking the real, $R_{ex} = -Re(E_1) - R_2^A$, and imaginary, $\delta_{ex} = Im(E_1)$, components of the smaller eigenvalue E_1 of the 2×2 matrix on the right-hand side of Eq. 1, leads to

$$R_{ex} = k_a \frac{k_b\Delta R + \Delta R^2 + \Delta\omega^2}{(k_b + \Delta R)^2 + \Delta\omega^2} \quad (2)$$

$$\delta_{ex} = k_a \frac{k_b\Delta\omega}{(k_b + \Delta R)^2 + \Delta\omega^2} \quad (3)$$

where $\Delta R = R_2^B - R_2^A$. These expressions were initially derived by Anet and Basus (1969) in the limit where $\Delta R = 0$, and later in a more general form by Skrynnikov et al. (2002). We denote the component of R_{ex} that 'survives' in the absence of chemical shift differences between states A and B ($\Delta\omega = 0$) and arises from large differences between the transverse spin relaxation rates R_2^A and R_2^B (large ΔR) as 'lifetime line broadening' or ΔR_2 given by,

$$\Delta R_2 = \frac{k_a\Delta R}{k_b + \Delta R} \quad (4)$$

As we focus here on exchanging systems where $R_2^B >> R_2^A$ and $k_b >> k_a$, we can write that

$$\Delta R_2 \approx \frac{k_a}{1 + (k_{ex}/R_2^B)} \quad (5)$$

where the exchange rate $k_{ex} = k_b + k_a \approx k_b$. A plot of ΔR_2 in units of k_a versus the ratio (k_{ex}/R_2^B) is shown in Fig. 1.

It is immediately evident from Eq. 5 and the plot in Fig. 1 that when exchange is fast on the transverse relaxation time scale $(k_{ex}/R_2^B >> 1)$, $\Delta R_2 \approx p_B R_2^B$; and when exchange is slow relative to the transverse relaxation rate $(k_{ex}/R_2^B << 1)$, $\Delta R_2 \approx k_a$. Experimentally, lifetime line-broadening (ΔR_2) is easily measured as the difference between transverse spin relaxation rates in the presence and absence of exchange under conditions where the contributions to R_{ex} arising from a finite (non-zero) value of $\Delta\omega$ are minimized (e.g. by using $R_{1\rho}$ measurements with strong on-resonance spin-lock fields). Therefore, any detailed investigation of exchange, in a biological system involving a large molecular weight

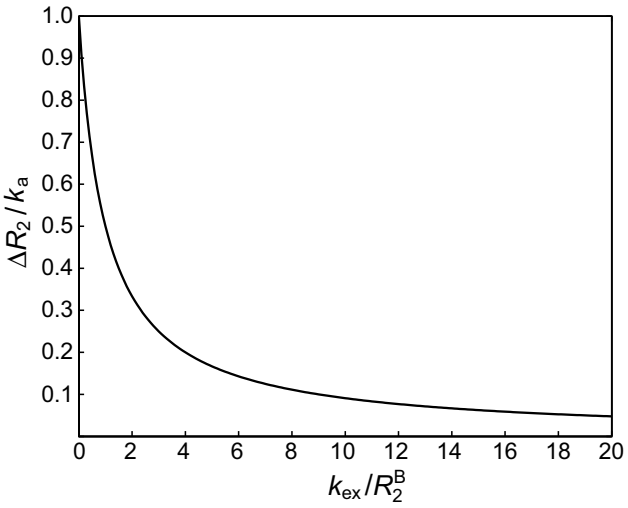

Fig. 1 Plot of $\Delta R_2/k_a$ (y-axis) versus k_{ex}/R_2^B (x-axis). The value of $\Delta R_2/k_a$, spanning a range from 0 to 1, is a measure of the exchange regime in relation to the time-scale of transverse relaxation

component, usually starts with the measurement of ΔR_2 as a function of controllable experimental parameters such as concentration, temperature and the strength of the static magnetic field.

The exchange regime on the relaxation time-scale (generally, not known *a-priori* for a given system in the absence of prior information on the rate constants) can be established from the dependence of ΔR_2 on the strength of the static magnetic (spectrometer) field B_0. The effect of B_0 on R_2^B is easily predictable from nuclear spin relaxation theory (Abragam 1961). The analysis below pertains almost exclusively to backbone ^{15}N nuclei in proteins as their sizable chemical shift anisotropy (CSA; ~ − 160 to 170 ppm) ensures that substantial (and predictable) changes in $^{15}\mathrm{N} - R_2^B$ accompany changes in B_0. Following the analysis of Millet et al. (2000) and Vallurupalli et al. (2011) of the dependence of R_{ex} and δ_{ex} on B_0, it is straightforward to show that,

$$\frac{d \ln \Delta R_2}{d \ln R_2^B} = \alpha \approx \frac{1}{1 + (R_2^B / k_{ex})} \tag{6}$$

where $0 \le \alpha \le 1$. From Eq. 6, it follows that for small changes in R_2^B and the static field, ΔB,ΔR_2 measured at a higher magnetic field $\left(\Delta R_2^{B_0+\Delta B}\right)$ is related to that measured at the lower field $\left(\Delta R_2^{B_0}\right)$ via the relationship,

$$\frac{\Delta R_2^{B_0+\Delta B}}{\Delta R_2^{B_0}} \approx n^{\alpha} \tag{7}$$

where n is a factor by which R_2^B is predicted to increase theoretically (e.g. ~ 1.3 between 900 and 600 MHz, and ~ 1.2 between 800 and 600 MHz for ^{15}N nuclei of the protein backbone), and the exchange regime is determined by the value of the exponent $\alpha = \ln\left(\Delta R_2^{B_0+\Delta B} \Big/ \Delta R_2^{B_0}\right) \Big/ \ln n$. Thus, the ratio of experimental ΔR_2 values (or their averages for different residues in a protein) measured at two spectrometer fields allows one to establish the exchange regime via the relationship in Eq. 7. Three regimes can be distinguished in this regard: (1) if the ratio, n^{α}, is equal or close to 1, $\Delta R_2 \approx k_a$ (slow exchange on the transverse relaxation time-scale, $k_{ex}/R_2^B << 1$); (2) if the ratio is close to the factor n, exchange is fast relative to transverse relaxation rates, $k_{ex}/R_2^B >> 1$; and (3) if the ratio adopts an intermediate value ($< n$ and > 1), the exchange rate k_{ex} is comparable to R_2^B (intermediate exchange regime on the transverse relaxation time scale with $R_2^B/k_{ex} = \alpha^{-1} - 1$). Further, although all the parameters of exchange cannot be determined unambiguously from the field-dependence of ΔR_2, even if the measurements are performed at more than two spectrometer fields, the forward rate constant k_a in the intermediate exchange regime (case 3 above) can be estimated from ΔR_2 recorded at two fields using the following relationship,

$$k_a = \frac{(n-1)\Delta R_2^{B_0} \Delta R_2^{B_0+\Delta B}}{n\Delta R_2^{B_0} - \Delta R_2^{B_0+\Delta B}} \tag{8}$$

where average values of ΔR_2 over all residues of a protein can be used. Equation 8 provides a means of estimating the value of k_a in the intermediate exchange regime from ΔR_2 data acquired at two spectrometer fields even in the absence of other experimental information.

DEST spectroscopy and associated NMR techniques

To characterize the kinetics of an exchanging system in detail, ΔR_2 measurements are usually combined with analysis of DEST profiles (Fawzi et al. 2010, 2011). DEST experiments involve the application of off-resonance radiofrequency (RF) radiation at a series of offsets from the resonance positions of the directly observable state A in order to saturate the nuclei of the large, spectroscopically invisible ('dark') state B. The magnetization is then transferred from the (partially) excited 'dark' state to the major, observable state A via exchange. Intensities of the NMR cross-peaks of the major visible species obtained at each offset frequency are subsequently normalized to those obtained without saturation or very far off-resonance where even the 'dark' state is not excited. The acquisition of such intensity profiles as a function of offset frequencies both up-field and down-field of the frequency range of the observable spectrum, is usually carried out at two or more RF saturation field strengths, which are chosen to maximize the broadening of the profiles in the presence of exchange while ensuring minimal saturation of cross-peaks in the absence of exchange. DEST profiles are commonly analysed via numerical integration of a set of homogeneous Bloch–McConnell differential equations (McConnell 1958; Helgstrand et al. 2000) (represented by a 7×7 matrix for a 2-state system), as no analytical expressions exist for the general case of exchange saturation transfer. Simultaneous analysis of DEST/ΔR_2 data allows the kinetic parameters of exchange, as well as the values of R_2^B, to be determined unambiguously under conditions where $R_2^B > \omega_1$ (the strength of the RF saturation field applied to the resonances of the 'dark' state). This was the case in the initial applications of the DEST/ΔR_2methodology to studies of early stages of amyloid aggregation (Fawzi et al. 2010, 2011). Below, we provide a brief description of the limitations of the DEST/ΔR_2 approach in cases when the above condition is not fulfilled, namely for intermediate values of R_2^B lying the range between ~ 500 and 5000 s^{-1} and therefore either smaller than

or comparable to the strength of the saturation fields employed in the DEST experiments.

Although the equations derived by Baldwin and Kay (2013) for $R_{1\rho}$, in the case where $R_2^B > R_2^A$, can be used to reproduce DEST profiles, the expressions are bulky and give little insight into how the parameters of exchange and relaxation relate to one another. That is why we choose to draw an analogy with the recent work of Kay and co-workers (Yuwen et al. 2018), where the authors probed a slowly exchanging protein system via off-resonance $R_{1\rho}$ experiments. For a two-state exchanging system in the limit where the strength of the RF field $\omega_1 >> R_2^B; k_{ex}$, the evolution of magnetization, in the absence of chemical shift differences between the inter-converting species ($\Delta\omega = 0$), can be approximated by,

$$\frac{d}{dt}\begin{bmatrix} M^A \\ M^B \end{bmatrix} = -\begin{bmatrix} k_a & -k_b \\ -k_a & k_b + R_2^B \sin^2\theta \end{bmatrix}\begin{bmatrix} M^A \\ M^B \end{bmatrix} \tag{9}$$

where the notation of Eq. 1 is preserved, and θ is the angle between the spin-locked magnetization and the z-axis of the laboratory frame (Yuwen et al. 2018). The longitudinal relaxation rates of states A and B (R_1^A and R_1^B), as well as the transverse relaxation rate of state A, R_2^A, are assumed to be zero in this approximation. The solution of Eq. 9 is given by,

$$\begin{aligned} M^A(t) &= Ae^{\lambda_s t} + Be^{\lambda_f t} \\ M^B(t) &= Ce^{\lambda_s t} + De^{\lambda_f t} \end{aligned} \tag{10}$$

where the small ('slow') and large ('fast') eigenvalues, λ_s and λ_f, are,

$$\lambda_{f,s} = -\frac{1}{2}\left(k_{ex} + R_2^B \sin^2\theta \pm \sqrt{\left(k_{ex} + R_2^B \sin^2\theta\right)^2 - 4p_B k_{ex} R_2^B \sin^2\theta}\right) \tag{11}$$

Expressions for the terms A–D in Eq. 10 when $\Delta\omega = 0$, are given by,

$$\begin{aligned} A &= \lambda_f\left(1 - p_B\right)/\left(\lambda_f - \lambda_s\right) \\ B &= -\lambda_s\left(1 - p_B\right)/\left(\lambda_f - \lambda_s\right) \\ C &= p_B\left(\lambda_f + R_2^B \sin^2\theta\right)/\left(\lambda_f - \lambda_s\right) \\ D &= -p_B\left(\lambda_s + R_2^B \sin^2\theta\right)/\left(\lambda_f - \lambda_s\right) \end{aligned} \tag{12}$$

$-\lambda_s$ represents the effective relaxation rate measured as a function of offset. From Eqs. 9–11, it therefore follows that the contribution to the transverse relaxation rate arising from exchange, R_{ex}, in the limit of skewed populations $\left(p_B << p_A\right)$ is given by,

$$R_{ex} = -\lambda_s/\sin^2\theta \approx \left[\frac{1}{p_B R_2^B} + \frac{\sin^2\theta}{p_B k_{ex}}\right]^{-1} \tag{13}$$

Equation 9 and its solutions in Eqs. 10–12 are a good approximation to the full Bloch–McConnell equations in the limit $\omega_1 >> R_2^B; k_{ex}$ for the analysis of off-resonance $R_{1\rho}$ experiments where the magnetization is aligned ('locked') along the effective RF field for each value of the offset (angle θ).

In exchange saturation transfer experiments such as DEST, however, the magnetization is saturated during the relaxation period by application of a continuous RF field so that the angle between the magnetization and the z-axis of the laboratory frame becomes time-dependent. Nevertheless, the DEST profiles generated via the full set of Bloch–McConnell equations can be reproduced reasonably well using the expression for the $R_{1\rho}$ relaxation rate, $R_{1\rho} = R_1\cos^2\theta + R_{2,eff}\sin^2\theta$, where $R_{2,eff} = R_2^A + R_{ex}$ and R_{ex} is calculated using Eq. 13, provided that the transverse relaxation rates R_2^B are sufficiently large. To further illustrate this point, the differences in normalized intensities Δ between DEST profiles generated using the full set of Bloch–McConnell equations and those calculated from $R_{1\rho}$ rates using Eq. 13 for R_{ex} are shown in Fig. 2a. As might be expected, the largest differences Δ are localized at intermediate offset values, but even the latter become very small by absolute magnitude as the transverse relaxation rates of state B increase (Fig. 1a). Interestingly, the agreement between the DEST profiles does not deteriorate for faster rates of exchange as shown in Fig. 2b, where the maximal deviations (by absolute magnitude) between the two profiles are plotted as a function of $\log_{10}(R_2^B)$ for exchange rates ranging from 100 to 10,000 s^{-1}. Since, for the purposes of this discussion, we are mostly interested in 'intermediate' relaxation rates, that is $\log_{10}(R_2^B)$ values spanning a range between ~2.8 and ~3.8 where a shallow minimum of $|\Delta|_{max}$ is observed in Fig. 2b in the case of faster exchange, we can conclude that the simplified treatment represented by Eqs. 9 and 13 above serves our illustrative purposes.

Equation 13 is particularly useful in illustrating the limitations of DEST/ΔR_2 analysis for intermediate R_2^B rates because it shows that whereas the value of $k_a = p_B k_{ex}$ in the denominator of the right term can be determined from ΔR_2 data acquired at two spectrometer fields and/or the combination of ΔR_2 and DEST profiles, the product $p_B R_2^B$ in the denominator of the first term is the only quantity that can be determined with certainty from DEST/ΔR_2 analysis under condition where R_2^B is not much larger than the strength of the applied saturation field ω_1 (in rad s^{-1}).

Numerical simulations using synthetic DEST data at three RF saturation fields in combination with ΔR_2 data at two spectrometer fields, confirm that as the value of R_2^B increases beyond the highest of the ω_1 fields employed in DEST measurements, the limitation of the DEST/ΔR_2 approach described above slowly disappears, i.e. accurate values of p_B and R_2^B can be extracted at the same time from the data

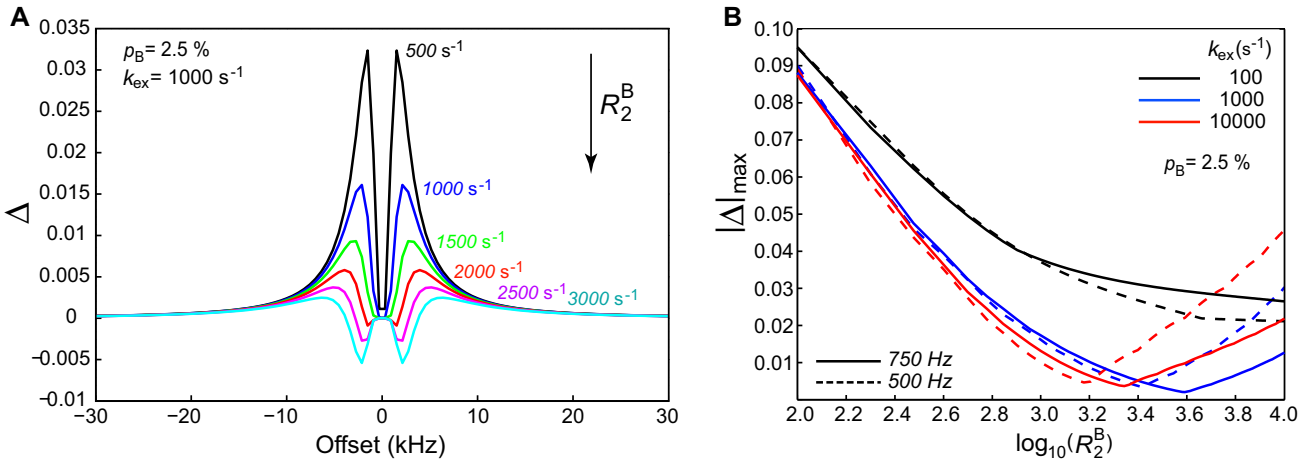

Fig. 2 **a** Difference (Δ) between normalized intensities of DEST profiles (scaled between 0 and 1) calculated using the full Bloch–McConnell equations and those calculated using Eq. 13 for a set of R_2^B values ranging from 500 to 3,000 s^{-1}. The exchange parameters used are: $p_B = 2.5\%$ and $k_{ex} = 1000$ s^{-1}.The plots are color-coded according to R_2^B values as indicated on the plot. **b** Maximal (by absolute magnitude) deviations $|\Delta|_{max}$ (*y*-axis) between the differences of the DEST profile calculated as in (**a**) plotted versus $\log_{10}(R_2^B)$ (*x*-axis) for three regimes of exchange, color-coded as indicated on the plot. Dashed and solid lines in all exchange regimes correspond to DEST RF saturation field of 500 and 750 Hz, respectively. p_B is fixed at 2.5% in all calculations

to within the uncertainties in the fitted parameters without resort to other/additional NMR experimental observables.

The approach used to de-correlate p_B and R_2^B for intermediate R_2^B values will depend upon the exchange regime on the transverse relaxation time-scale. For slow exchange $\left(k_{ex}/R_2^B < 1\right)$, another observable quantity introduced by Kay and co-workers (Yuwen et al. 2018) can be used. This experimental observable, denoted as C_{fast}, relates to the fractional contribution of the fast decaying component of $R_{1\rho}$ relaxation to the total signal intensity: namely, (B + D) in Eq. 10, with the sum of all eigenvectors (A + B + C + D) normalized to unity. From Eq. 10, the decay of 'spin-locked' magnetization for each state in $R_{1\rho}$ experiments is inherently biphasic. When care is taken in $R_{1\rho}$ measurements to carefully equilibrate magnetization before and after each relaxation period ('spin-lock' element), the magnetizations of the A and B states after each relaxation period are given by, $M_{eq}^A(T) = (1 - p_B)\left[M^A(T) + M^B(T)\right]$ and $M_{eq}^B(T) = p_B\left[M^A(T) + M^B(T)\right]$, where T is the duration of relaxation delay. The C_{fast} component can then be reliably estimated from extrapolation of the $R_{1\rho}$ decay to zero time provided that normalization of signal intensities is performed relative to those measured in the absence of a relaxation period (i.e. at $T = 0$). The latter correspond to (A + B + C + D) in Eq. 10. The measurement of a single C_{fast} value per residue at or close to on-resonance frequency is sufficient to de-correlate p_B and R_2^B (Ceccon et al. 2018a). On resonance ($\sin\theta = 1$ in Eqs. 9–12), C_{fast} reaches its maximal value, denoted as C_{fast}^{max} in the following. For skewed populations ($p_B << p_A$), C_{fast}^{max}can be simplified to,

$$C_{fast}^{max} = \frac{p_B}{1 + \left(k_{ex}/R_2^B\right)^2 + \left(2k_{ex}/R_2^B\right)\left(1 - p_B\right)} \approx \frac{p_B}{\left(1 + \frac{k_{ex}}{R_2^B}\right)^2} \quad (14)$$

Equation 14 shows that C_{fast}^{max} is directly proportional to p_B. Thus, provided that $k_{ex}/R_2^B < 1$, C_{fast}^{max} serves as a good measure of the population of the bound state p_B, even if only a single (on-resonance) measure of C_{fast} is available. Inclusion of an additional term that accounts for C_{fast}^{max} data into the DEST/ΔR_2 target function, then enables unambiguous determination of p_B (and therefore k_{off}), as well as the set of residue-specific R_2^B values (Ceccon et al. 2018a).

If, however, the ratio k_{ex}/R_2^B is significantly larger than unity (fast exchange on the transverse relaxation time-scale) or p_B is small (< ~ 1%), C_{fast}^{max} will decrease to unmeasurably low values (Eq. 14), and the application of other NMR techniques, such as the measurement of chemical exchange line-broadening R_{ex} (Eq. 2) and exchange-induced chemical shifts δ_{ex} (Eq. 3), is required to characterize the parameters of exchange unambiguously. The latter can be measured directly if the state of the system without exchange (state A only) is experimentally accessible or assessed indirectly from the dependence of the chemical shifts of state A on the spectrometer field (Skrynnikov et al. 2002), while the former is usually quantified via Carr-Purcell-Meiboom-Gill (CPMG) relaxation dispersion (Meiboom and Gill 1958; Palmer 2014) measured in a constant time manner (Mulder et al. 2000).

For two-site exchange the evolution of the magnetization vector $M = [M^A;M^B]^T$ in Eq. 1 (where T denotes

transposition) during the CPMG constant time period is represented by,

$$M(t) = (AA^*A^*A)^{ncyc}M(0) \tag{15}$$

where $A = \exp(-\tilde{R}\tau_{CP}/2)$; A^* is the complex conjugate of A, $ncyc$ is the number of CPMG cycles employed, τ_{CP} is the time-period between two consecutive 180° pulses in the CPMG pulse train, and $\tilde{R}$ is the 2×2 matrix on the right-hand side of Eq. 1. Although this approach adds additional parameters to the analysis in the form of chemical shift differences $\Delta\omega$ (note that neither DEST nor lifetime line-broadening ΔR_2 data are sensitive to differences in chemical shifts between the states), the significantly different dependence of R_{ex} and δ_{ex} on the parameters of exchange (*cf.* Equations 2 and 3; see also (Vallurupalli et al. 2011)), and the use of R_{ex} and δ_{ex} in combination with DEST and ΔR_2 data, solves the problem of correlated parameters in DEST/ΔR_2 analysis and provides $\Delta\omega$ values (Libich et al. 2013). Of note, CPMG relaxation dispersions are used in this type of analysis in a somewhat unconventional way by allowing the values of R_2^B to be variable parameters in the fit. Numerical simulations of fits to synthetic DEST data at three RF fields, ΔR_2 data and CPMG profiles at two spectrometer fields, and δ_{ex} at the highest spectrometer field, show that the minimal $|\Delta\omega|$ value required for reliable extraction of exchange parameters is quite small, on the order of 0.8–1.0 ppm for ^{15}N nuclei. The larger are the values of ^{15}N$-|\Delta\omega|$, the greater is the accuracy of the fitted exchange parameters.

In this context, we note that it may be tempting to forgo the measurement of ΔR_2 altogether as CPMG relaxation dispersion profiles contain the same information in the limit of fast pulsing (at high CPMG frequencies). We therefore investigated this issue in more detail. The general analytical solution for the measured effective relaxation rate $R_{2,eff}$ in a two-site exchanging system is given by the Carver-Richards equation (Carver and Richards 1972; Davis et al. 1994). It is straightforward to show that in the limit where $\Delta\omega = 0$ (no chemical shift differences between states A and B), the Carver-Richards equation reduces to the expression for the effective relaxation rate equal to $R_2^A + \Delta R_2^{CR}$, where the superscript '*CR*' denotes 'Carver-Richards', and ΔR_2^{CR} is given by,

$$\Delta R_2^{CR} = \frac{1}{2}\left[\Delta R + k_{ex} - \left\{\Delta R^2 + k_{ex}^2 + 2\Delta R(k_b - k_a)\right\}^{1/2}\right] \tag{16}$$

The expression in Eq. 16 is equivalent to ΔR_2 calculated from the exact solution of Eq. 1 in the $\Delta\omega = 0$ limit, i.e. equal to $-Re(E_1) - R_2^A$ where E_1 is the smaller eigenvalue of the matrix in Eq. 1. It is important, however, to realise that since CPMG relaxation dispersions are recorded in a constant-time manner, the resulting $R_{2,eff}$ values will involve a (small) correction. The analytical form of this correction in the general case was derived earlier by Baldwin (2014). Here, we are concerned with the fact that this small correction adopts a finite (non-zero) value even in the limit where $\Delta\omega = 0$. In this limit, using the expressions of Baldwin (2014), this correction, which we denote in the following by $\delta\Delta R_2^{CPMG}$, is given by,

$$\delta\Delta R_2^{CPMG} = -\frac{\ln Q}{T_{relax}} \tag{17}$$

where $Q = \frac{1}{2}\left(1 + e^{-T_{relax}\sqrt{\varepsilon}} + (\Delta R + k_{ex})\left(1 - e^{-T_{relax}\sqrt{\varepsilon}}\right)/\sqrt{\varepsilon}\right)$; T_{relax} is the duration of the constant time period used in the CPMG experiments; and $\varepsilon = (\Delta R + k_b - k_a)^2 + 4k_ak_b = (\Delta R + k_{ex})^2 - 4\Delta R p_B k_{ex}$. The correction $\delta\Delta R_2^{CPMG}$ is very small under most circumstances, almost inversely proportional to the duration of the CPMG constant-time period, and dependent mostly on the fractional population of the minor state (p_B). $\delta\Delta R_2^{CPMG}$ is plotted as a function of p_B for exchange rates ranging from 200 to 3500 s^{-1} with $R_2^B = 900$ s^{-1} in Fig. 3. The function in Eq. 17 can be shown to have a minimum (the largest value of the correction achieved by absolute magnitude) when $k_{ex}/R_2^B \approx 1$. That is why the lowest curve (shown in magenta in Fig. 3) corresponds to $k_{ex} \approx R_2^B$ (see also the inset in Fig. 3 where $\delta\Delta R_2^{CPMG}$ is plotted as a function of k_{ex} for $p_B = 10\%$). Numerical simulations of $R_{2,eff}$ rates, obtained from constant-time CPMG relaxation dispersion measurements for two-site exchange in the $\Delta\omega = 0$ limit using the evolution law in Eq. 15, are fully consistent with those obtained from the relationship, $R_{2,eff} = R_2^A + \Delta R_2 + \delta\Delta R_2^{CPMG}$, where

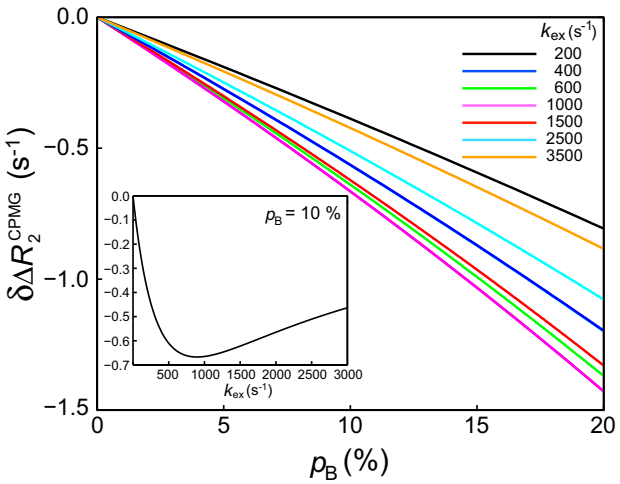

Fig. 3 Plot of $\delta\Delta R_2^{CPMG}$(s^{-1}) as a function of the population of the minor state, p_B, for exchange rates (k_{ex}) ranging from 200 to 3,500 s^{-1}, $R_2^B = 900$ s^{-1}, and $T_{relax} = 40$ ms. Equation 17 was used for all calculations of $\delta\Delta R_2^{CPMG}$. The curves are color-coded according to the value of k_{ex} as indicated in the plot. The inset shows a plot of $\delta\Delta R_2^{CPMG}$ as a function of k_{ex} for $p_B = 10\%$ and $R_2^B = 900$ s^{-1}

$\delta\Delta R_2^{CPMG}$ is calculated using Eq. 17. Overall, the values of $\delta\Delta R_2^{CPMG}$ are likely to be well below the experimental uncertainties in CPMG relaxation dispersion measurements unless the 'dark' state B is highly populated ($\geq \sim 10$–15%). We note, however, that much higher accuracy for ΔR_2 values can be achieved if the latter are measured separately via dedicated $R_{1\rho}$ experiments. It is therefore generally not advisable to rely on CPMG relaxation dispersion data for the measurement of ΔR_2.

Applications to exchanging systems involving high-molecular-weight species

In this section we present a concise survey of the applications of DEST/ΔR_2methodology for a number of interesting biological systems with special emphasis on the quantitative aspects of extraction of kinetic and spin relaxation parameters in different regimes of chemical exchange.

The first applications of DEST/ΔR_2 methodology focussed on the early stages of self-aggregation of amyloid β (Aβ) peptides, where the transverse relaxation rate R_2^B of the dark state, corresponding to Aβ proto-fibrillar assemblies, was very large, typically reaching tens of thousands per second. Hence, $R_2^B >> \omega_1$, where ω_1 is the strength of the applied RF field in DEST experiments, typically not exceeding ~ 4700 rad s^{-1} (Fawzi et al. 2010, 2011). Exchange between Aβ free in solution and on the surface of Aβ proto-fibrils is slow on the transverse relaxation time scale ($k_{ex}/R_2^B << 1$) and, hence, ΔR_2 is independent of either spectrometer field or type of nucleus: $\Delta R_2 \approx k_{on}^{app}$, where k_{on}^{app} is the 'apparent' pseudo-first-order association rate constant. In terms of our analysis above, this corresponds to a value of α in Eq. 7 close to 0. In this exchange regime, the very high transverse relaxation rate of the dark state ensured that accurate values of the kinetic parameters of exchange and R_2^B could be obtained reliably from the combined analysis of DEST profiles acquired at two RF field strengths and ΔR_2 profiles acquired at two spectrometer fields.

Subsequently, the DEST/ΔR_2 methodology was applied to exchanging systems with $^{15}N - R_2^B$ rates smaller than ω_1. Examples include binding of Aβ40 (Libich et al. 2013) and Aβ42 (Wälti et al. 2018) to the 800-kDa chaperonin GroEL. In these two cases, exchange (binding) occurs on a much faster time-scale ($k_{ex}/^{15}N - R_2^{B,600}$ ranges from ~ 3 to ~ 16 depending on the residue) leading to a steep dependence of ΔR_2 on the type of nucleus probed (backbone amide ^1H relaxation rates compared to those of backbone ^{15}N nuclei) as well as spectrometer field. The value of α calculated from Eq. 6 ranges from 0.75 to 0.94, which compares well with the corresponding values of 0.65 and 1.0 calculated using Eq. 7 from the smallest and largest ΔR_2 ratios, respectively, at 900 and 600 MHz spectrometer fields. In these systems, simultaneous extraction of the kinetic parameters of exchange (namely, the dissociation rate constants of the complexes, k_{off}, and consequently the population of the dark/bound state, p_B) together with the rates R_2^B, is no longer possible without additional information obtained from CPMG relaxation dispersion experiments and/or exchange-induced chemical shift measurements. Without these additional experiments, the DEST/ΔR_2 data only, acquired on an exchanging system with $R_2^B < \omega_1$, are not sufficient for determination of p_B (and hence k_{off}) and R_2^B rates independently, even if high-quality DEST profiles at several RF field strengths are available. Although chemical shift differences between free and GroEL-bound forms of Aβ40 and Aβ42 are quite small (not exceeding ~ 1 and ~ 0.1 ppm for $^{15}N/^{13}C\alpha$ and ^1H_N nuclei, respectively), the shifts induced by these differences together with CPMG relaxation dispersion and DEST/ΔR_2 data proved sufficient for unambiguous determination of all parameters of exchange.

The same correlation between kinetic (p_B and k_{off}) and relaxation (R_2^B) parameters of exchange was described in our studies of the truncated VPL-mutant of the Fyn-SH3 domain ($FynSH3^{Mut}\Delta 56$) bound to GroEL (Libich et al. 2017), where the field-dependence of $^{15}N - \Delta R_2$ yields a value of α in Eq. 7 of ~ 0.27, indicating that binding to GroEL proceeds in the slow-to-intermediate regime on the transverse relaxation time-scale $\left(^{15}N - R_2^{B,600}/k_{ex} = \alpha^{-1} - 1 \approx 2.7\right)$. The ^{15}N-DEST/ΔR_2 data of $FynSH3^{Mut}\Delta 56$ in the presence of GroEL could be fit equally well for a continuum of $\{p_B;R_2^B\}$ combinations (Libich et al. 2017), indicating that a strong correlation exists between these two parameters. De-correlation of p_B from R_2^B was achieved in this case by assuming a certain average transverse ^{15}N spin relaxation rate in the bound state, $\left\langle ^{15}N - R_2^B \right\rangle$, based on the molecular weight of the $FynSH3^{Mut}\Delta 56$-GroEL complex (~ 950 s^{-1} at 900 MHz and 10 °C for a well-ordered N–H bond vector). We note that the earlier study of the folding-unfolding equilibrium of the full-length Fyn-SH3 VPL-mutant, $FynSH3^{VPL}$ in the free and GroEL-bound states (Libich et al. 2015) (characterized by intermediate-to-fast binding, with the field-dependence of $^{15}N - \Delta R_2$ corresponding to α in the range ~ 0.6–0.8), was largely driven by quantitative analysis of (and the observed differences in) CPMG relaxation dispersion profiles in the presence (4-state model) and absence (2-state model) of GroEL. Therefore, no correlations between $^{15}N - R_2^B$ rates and the population(s) of the GroEL-bound state(s) were observed in this work. In another recent study, the binding of two huntingtin exon-1 peptides, htt^{NT} and $htt^{NT}Q_7$, to ~ 30 nm-diameter small unilamellar lipid vesicles (SUVs; $^{15}N - R_2^B \sim 2{,}000$ s^{-1} at 600 MHz) occurs in a very slow exchange regime $\left(k_{ex}/^{15}N - R_2^B \sim 0.1\right)$ (Ceccon et al. 2018a). Not surprisingly, $^{15}N - \Delta R_2$ profiles in this case do not show any traces of field-dependence ($\alpha \sim 0$). The low

value of the $\left(K_{ex}/^{15}\mathrm{N}-R_2^B\right)$ ratio ensures that reliable estimates of p_B can be obtained from the measurements of C_{fast}^{max} (see Eq. 14). To amplify the value of C_{fast}^{max} ~two-fold, two spin-lock periods were used in the total relaxation delay, each preceded and followed by a magnetization equilibration delay $\tau_{eq} \geq 2/k_{ex}$ (Yuwen et al. 2018). In this instance, exchange is very slow on the transverse relaxation timescale, and the measurements of C_{fast}^{max} for htt^{NT} and $htt^{NT}Q_7$ peptides in the presence of SUVs proved indispensable for de-correlating the kinetic (p_B and k_{off}) and relaxation ($^{15}\mathrm{N}$–R_2^B) parameters of exchange. The inclusion of an additional term that accounts for C_{fast}^{max} data into the DEST/ΔR_2 target function, enabled unambiguous determination of p_B and k_{off} for htt^{NT} and $htt^{NT}Q_7$ binding to SUVs, as well as the set of residue-specific $^{15}\mathrm{N}$–R_2^B values, without compromising the quality of the fit to the DEST or ΔR_2 profiles (Ceccon et al. 2018a).

Acknowledgements This mini-review is dedicated to our colleague and long-time friend, Dr. Dennis A. Torchia on the occasion of his 80th birthday. This work was supported by funds from the Intramural Program of the National Institute of Diabetes and Digestive and Kidney Diseases, National Institutes of Health (G.M.C.).

References

Abragam A (1961) Principles of nuclear magnetism. Clarendon Press, Oxford

Anet FAL, Basus VJ (1969) Limiting equations for exchange broadening in two-site nmr systems with very unequal populations. J Magn Reson 32:339–343

Anthis NJ, Clore GM (2015) Visualizing transient dark states by NMR spectroscopy. Q Rev Biophys 48:35–116

Baldwin AJ (2014) An exact solution for $R_{2,eff}$ in CPMG experiments in the case of two site chemical exchange. J Magn Reson 244:114–124

Baldwin AJ, Kay LE (2013) A$R_{1\rho}$ expression for a spin in chemical exchange between two sites with unequal transverse relaxation rates. J Biomol NMR 55:211–218

Carver JP, Richards RE (1972) General two-site solution for chemical exchange produced dependence of T_2 upon Carr–Purcell pulse separation. J Magn Reson 6:89–105

Ceccon A, Lelli M, D'Onofrio M, Molinari H, Assfalg M (2014) Dynamics of a globular protein adsorbed to liposomal nanoparticles. J Am Chem Soc 136:13158–13161

Ceccon A, Clore GM, Tugarinov V (2016a) Towards interpretation of intermolecular paramagnetic relaxation enhancement outside the fast exchange limit. J Biomol NMR 66:1–7

Ceccon A, Tugarinov V, Bax A, Clore GM (2016b) Global dynamics and exchange kinetics of a protein on the surface of nanoparticles revealed by relaxation-based solution NMR spectroscopy. J Am Chem Soc 138:5789–5792

Ceccon A, Tugarinov V, Boughton AJ, Fushman D, Clore GM (2017) Probing the binding modes of a multidomain protein to lipid-based nanoparticles by relaxation-based NMR. J Phys Chem Lett 8:2535–2540

Ceccon A, Clore GM, Tugarinov V (2018a) Decorrelating kinetic and relaxation parameters in exchange saturation transfer NMR: a case study of N-terminal huntingtin peptides binding to unilamellar lipid vesicles. J Phys Chem B 122:11271–11278

Ceccon A, Schmidt T, Tugarinov V, Kotler SA, Schwieters CD, Clore GM (2018b) Interaction of huntingtin exon-1 peptides with lipid-based micellar nanoparticles probed by solution NMR and Q-band pulsed EPR. J Am Chem Soc 140:6199–6202

Ceccon A, Tugarinov V, Clore GM (2019) TiO_2 nanoparticles catalyze oxidation of huntingtin exon 1-derived peptides impeding aggregation: a quantitative NMR study of binding and kinetics. J Am Chem Soc 141:94–97

Conicella AE, Fawzi NL (2014) The C-terminal threonine of Aβ43 nucleates toxic aggregation via structural and dynamical changes in monomers and protofibrils. Biochemistry 53:3095–3105

Davis DG, Perlman ME, London RE (1994) Direct measurements of the dissociation-rate constant for inhibitor-enzyme complexes via the T_1 and T_2(CPMG) methods. J Magn Reson Ser B 104:266–275

Egner TK, Naik P, Nelson NC, Slowing II, Venditti V (2017) Mechanistic insight into nanoparticle surface adsorption by solution NMR spectroscopy in an aqueous gel. Angew Chem Int Ed Engl 56:9802–9806

Fawzi NL, Ying J, Torchia DA, Clore GM (2010) Kinetics of amyloid β monomer-to-oligomer exchange by NMR relaxation. J Am Chem Soc 132:9948–9951

Fawzi NL, Ying J, Ghirlando R, Torchia DA, Clore GM (2011) Atomic-resolution dynamics on the surface of amyloid-β protofibrils probed by solution NMR. Nature 480:268–272

Fawzi NL, Ying J, Torchia DA, Clore GM (2012) Probing exchange kinetics and atomic resolution dynamics in high-molecular-weight complexes using dark-state exchange saturation transfer NMR spectroscopy. Nat Protoc 7:1523–1533

Fawzi NL, Libich DS, Ying J, Tugarinov V, Clore GM (2014) Characterizing methyl-bearing side chain contacts and dynamics mediating amyloid β protofibril interactions using $^{13}C_{methyl}$-DEST and lifetime line broadening. Angew Chem Int Ed Engl 53:10345–10349

Helgstrand M, Hard T, Allard P (2000) Simulations of NMR pulse sequences during equilibrium and non-equilibrium chemical exchange. J Biomol NMR 18:49–63

Libich DS, Fawzi NL, Ying J, Clore GM (2013) Probing the transient dark state of substrate binding to GroEL by relaxation-based solution NMR. Proc Natl Acad Sci USA 110:11361–11366

Libich DS, Tugarinov V, Clore GM (2015) Intrinsic unfoldase/foldase activity of the chaperonin GroEL directly demonstrated using multinuclear relaxation-basedNMR. Proc Natl Acad Sci USA 112:8817–8823

Libich DS, Tugarinov V, Ghirlando R, Clore GM (2017) Confinement and stabilization of Fyn SH3 folding intermediate mimetics within the cavity of the chaperonin GroEL demonstrated by relaxation-based NMR. Biochemistry 56:903–906

McConnell HM (1958) Reaction rates by nuclear magnetic resonance. J Chem Phys 28:430–431

Meiboom S, Gill D (1958) Modified spin-echo method for measuring nuclear relaxation times. Rev Sci Instrum 29:688–691

Millet O, Loria PJ, Kroenke CD, Pons M, Palmer AG (2000) The static magnetic field dependence of chemical exchange linebroadening defines the NMR chemical shift time scale. J Am Chem Soc 122:2867–2877

Mulder FA, Hon B, Muhandiram DR, Dahlquist FW, Kay LE (2000) Flexibility and ligand exchange in a buried cavity mutant of T4 lysozyme studied by multinuclear NMR. Biochemistry 39:12614–12622

Palmer AG (2014) Chemical exchange in biomacromolecules: past, present, and future. J Magn Reson 241:3–17

Skrynnikov NR, Dahlquist FW, Kay LE (2002) Reconstructing NMR spectra of "invisible" excited protein states using HSQC and HMQC experiments. J Am Chem Soc 124:12352–12360

Vallurupalli P, Bouvignies G, Kay LE (2011) Increasing the exchange time-scale that can be probed by CPMG relaxation dispersion NMR. J Phys Chem B 115:14891–14900

Wälti MA, Steiner J, Meng F, Chung HS, Louis JM, Ghirlando R, Tugarinov V, Nath A, Clore GM (2018) Probing the mechanism of inhibition of amyloid-β(1–42)-induced neurotoxicity by the chaperonin GroEL. Proc Natl Acad Sci USA 115:E11924–E11932

Yuwen T, Brady JP, Kay LE (2018) Probing conformational exchange in weakly interacting, slowly exchanging protein systems via off-resonance $R_{1\rho}$ experiments: Application to studies of protein phase separation. J Am Chem Soc 140:2115–2126